Chemosphere 241 (2020) 125068

Contents lists available at ScienceDirect

Chemosphere

journal homepage: www.elsevier.com/locate/chemosphere

Enhanced antifouling performance of PVDF ultrafiltration membrane by blending zinc oxide with support of graphene oxide nanoparticle

Sivasankaran Ayyaru, Ta Tuan Linh Dinh, Young-Ho Ahn*

Department of Civil Engineering, Yeungnam University, Gyeongsan 38541, South Korea

HIGHLIGHTS

- A hydrophilic additive, association of graphene oxide (GO) and ZnO, was prepared.
- The influence of hydrophilicity of GO-ZnO on the PVDF membrane was examined.
- The water flux of the GO-ZnO/PVDF membrane showed 48% higher than that of bare PVDF.
- The GO-ZnO membrane showed lower Rir fouling resistance of 7.21% than GO (15.09%).
- The anti-fouling properties PVDF improved by hydrophilicity of the GO-ZnO composite.

ARTICLE INFO

Article history:
Received 12 August 2019
Received in revised form
2 October 2019
Accepted 5 October 2019
Available online 9 October 2019

Handling editor: Dr Y Yeomin Yoon

Keywords:
Nanocomposite additive
GO-ZnO nanocomposite
Polyvinylidene fluoride (PVDF)
Ultrafiltration
Antifouling

ABSTRACT

This paper reports a novel nanocomposite additive for a polyvinylidene fluoride (PVDF) membrane with high hydrophilicity through the association of graphene oxide (GO) and ZnO. The influence of the hydrophilicity of GO-ZnO on the PVDF membrane was examined on different GO-ZnO loadings. The porosity and wettability (or hydrophilicity) of the membrane were improved significantly by blending GO-ZnO nanocomposite. In addition, the water flux of the GO-ZnO/PVDF membrane was 48% higher than that of bare PVDF, and the anti-fouling properties of this modified membrane were also improved. The irreversible fouling ratio (Rir) of bovine serum albumin (BSA) was reduced substantially with increasing the loading of GO-ZnO nanocomposite. The lowest irreversible fouling ratio (7.21%) was obtained for the membrane containing 0.2 wt % GO-ZnO of the nanocomposite (M6). GO-ZnO modification PVDF membranes were assumed to reduce the affinity between membrane and BSA foulant, which improved the anti-fouling properties PVDF membrane. In the activated sludge flux test, the membrane containing GO-ZnO in the polymer matrix had a higher flux than that of the bare PVDF membrane. The effluent quality after the composite membrane (0.6 NTU) was stable, indicating that the composite membrane can be used for practical applications Overall, the properties of the PVDF membrane were improved after modification due to hydrogen bonding or the hydrophilicity of the GO-ZnO nanocomposite.

© 2019 Elsevier Ltd. All rights reserved.

1. Introduction

In the recent decades, overpopulation has resulted in a shortage of clean water. Therefore, many solutions, such as adsorption, ion exchange, advanced oxidation, and membrane separation process, was applied to overcome this problem (Warsinger et al., 2016). In these solutions, the membrane separation process represents the most advanced technology for water and wastewater treatment because of its small footprint, reduced sludge production through maintaining a high biomass concentration in the bioreactor with excellent effluent quality and automated operation and high efficiency (Chang et al., 2002; Wang et al., 2012; Chang et al., 2014; Zhang et al., 2013). Ultrafiltration (UF) has attracted increasing attention in both water and wastewater treatment. With the principal features of porosity, permeability, hydrophilicity, and chemical resistance, UF allows perfect separation between water and contaminants, such as pathogenic protozoa, and small particles (Howe KJ, 2002; Chang et al., 2014; Lai et al., 2014; Ayyaru et al., 2019).

Recently, polyvinylidene fluoride (PVDF) is a promising polymer to fabricate membranes with high mechanical strength, excellent thermal behavior, and high chemical resistance. Therefore, PVDF

* Corresponding author.
E-mail address: yhahn@ynu.ac.kr (Y.-H. Ahn).

https://doi.org/10.1016/j.chemosphere.2019.125068
0045-6535/© 2019 Elsevier Ltd. All rights reserved.

has been commercialized and become a popular membrane technology (Cao et al., 2006). On the other hand, its inherent hydrophobicity results in a decrease in water permeability as well as serious fouling. Fouling reduces the longevity of a membrane and increases the operating costs. Two key factors affect the fouling of PVDF membranes: the hydrophobic nature of the foulant, which allows the foulant to deposit easily on the membrane surface and adsorb at the pore wall; and the porous structure of the membrane (Zhao et al., 2012). Therefore, the adoption of advanced techniques could control the hydrophilicity and improve the fouling resistance of PVDF membranes (Qin et al., 2013; Chang et al., 2014).

Considerable efforts have been made to improve the hydrophilicity of the polymeric membrane. The solutions reported thus far include modifying the surface, blending the hydrophilic polymers and adding nanoparticles to the casting solution (Ayyaru and Ahn, 2018). In this regard, the appropriate addition of inorganic nanoparticles, e.g., Al_2O_3, TiO_2, SiO_2, Fe_3O_4, ZrO_2, ZnO, and $LiClO_4$, have attracted attention because of its extraordinary features (Bottino et al., 2002; Yan et al., 2006; Cui et al., 2010; Wei et al., 2011; Huang et al., 2012; Ayyaru and Ahn, 2018; Li et al., 2018). The hybrid inorganic nanoparticles membrane showed improved water flux, hydrophilicity, mechanical strength, rejection, and membrane surface formation. In contrast, remarkable negative effects still exist in the hybrid membrane. Nanoparticles tend to aggregate in the casting solution, which leads to imperfect pore formation and a less effective increase in the positive effects of membrane (Yang and Wang, 2006; Wu et al., 2008; J. Ma et al., 2013; Zhang et al., 2013). Hence, the selection of a nanoparticle should be as high as specific surface area, but the lower additive proportion (with low density, like corban nanotube (CNT) and graphene oxide (GO)) is important (Ayyaru and Ahn, 2017). In the recent research, the blending of GO in the membranes resulted in an astonishing improvement in membrane technology. By possessing abundant oxygen-containing functional groups (e.g., carboxyl, carbonyl, epoxy groups, and hydroxyl) and a single layer structure, GO is an extremely high aspect ratio, low density, and high strength material (Kim et al., 2007; Jiao et al., 2009; Wang et al., 2012; J. Zhang et al., 2013; Zhao et al., 2014). GO has a unique graphitized planar structure and a surface that can be functionalized easily. These characteristics play important roles in improving the contact area with the polymer matrix.

Wang et al. reported, improved water flux and antifouling of PVDF ultrafiltration membrane achived with addition of hydrophilic GO nanosheets inside (Wang et al., 2012). Zhang et al. showed that there was an improvement in water flux and antifouling at the PVDF-GO membrane compared to PVDF oxidized multi-walled carbon nanotube (OMWCNT) membranes (J. Zhang et al., 2013). On the other hand, the amphiphilic nature of GO inhibits the ability to improve its hydrophilicity (water uptake) on nanocomposite membranes. A hydrophobic pollutant (proteins) can be absorbed on the GO membrane surface (Ayyaru and Dharmalingam, 2011; Feng et al., 2013; Beydaghi et al., 2014; Feng et al., 2014). Mahlangu et al. examined the effects of incorporating a GO-ZnO blend in polyethersulfone (PES) membranes and investigated the trace organic compound (TOrC) removal in pharmaceutical wastewater. They reported that the GO-ZnO modification PES membranes reduce the interaction between the membrane and trace organic pollutants as well as the attraction between the membrane and foulant, which improve the trace organic rejection and anti-fouling properties (Mahlangu et al., 2017b). This was attributed to the reduced contact angles of the membranes after blending of the hydrophilic GO-ZnO material. However, the pure water flux was very low compared to other microfiltration and ultrafiltration membranes (Mahlangu et al., 2017a). Thus may be due the membrane synthesis approach of double-casting phase inversion (DCPI) method. Moreover, the GO-ZnO nanomaterial in PES not yet been reported in the common method of blending of nanoparticles in polymer matrix.

Zhang et al. investigated the PVDF/GO/ZnO composite membranes for photocatalytic activity of removal of organic dyes by preparing PVDF membrane as a carrier and zinc oxide (ZnO) as photo-catalyst and graphene (GO) as dispersant. They have observed that, the photocatalytic degradation rate of PVDF/GO/ZnO composite membranes for methylene blue (MB) reached 86.84% (Zhang et al., 2019). However, the water transport phenomena like pure water flux, pore size, porosity, antifouling, protein rejection have not been studied. Moreover, this study was mainly focused only photocatalystic activity of organic dye removal. They did not study for the filtration phenomena of PVDF/GO/ZnO composite membranes in the water filtration. (Zhang et al., 2019).

Zinc oxide (ZnO) is one of the metal oxide which has very good physico-chemical properties with antimicrobial activity (Moezzi et al., 2012). It has also been used as a photocatalyst to remove the organic pollutants in water and air (Li et al., 2012). Unquestionably, ZnO is best candidate to substitute TiO_2 in the solar cells due to its similar energy levels and high electron mobility (Zhao et al., 2018). Consequently, ZnO particles have been used in nanofluids for direct absorption solar collectors. With best optical properties of ZnO nanoparticles, the dispersion of particles is also vital for nanofluids applications. Of late, Bahng et al. proposed a kind of hedgehog particles (HP, composite of polystyrene and ZnO), which demonstrates the polar ZnO surfaces, is highly hydrophilic, they form tremendous dispersions in water and other hydrophilic solvents (Bahng et al., 2015).

Since, no studies have been conducted on GO-ZnO blend in PVDF membranes for membrane filtration previous applications. In this study, the GO surface was combined with ZnO to increase the hydrophilicity of the PVDF membranes and the antifouling properties were also advanced. The novelty in this manuscript lies in introducing GO-ZnO nanocomposite to PVDF in order to improve the performance of PVDF membrane for wastewater filtration. The surface of the nanocomposites was examined by Fourier transform infrared (FTIR) spectroscopy, X-ray photoelectron spectroscopy (XPS), X-ray powder diffraction (XRD), and scanning electron microscopy (SEM). The hybrid PVDF UF membranes were fabricated by phase inversion, and investigated by measuring the porosity and contact angle, and by scanning electron microscopy (SEM). The water permeation flux, water flux recovery, and fouling resistance are parameters that evaluate the membranes.

2. Methodology

2.1. Material

All chemicals used in the experiments were analytical grade. Graphite powder (Kanto Chemical Co., Inc., Japan) was used as the graphene oxide precursor. PVDF (Kynar 760), as the membrane material, was purchased from Arkema, France. Bovine serum albumin (BSA), N-methyl-2-pyrrolidone (NMP), polyvinylpyrrolidone (PVP), and zinc chloride ($ZnCl_2$) were obtained from KOSDAQ Company, Korea. Zinc chloride ($ZnCl_2$) and potassium permanganate ($KMnO_4$) were purchased from Duksan Pure Chemicals Company, Korea.

2.2. Synthesis GO

Graphene oxide was prepared using an improved method (Marcano et al., 2010). A solution of concentrated H_2SO_4/H_3PO_4 (360:40 ml) was prepared. Subsequently, 3 g of graphite powder was added with vigorous stirring followed by the slow addition of 18 g potassium permanganate. The reaction was performed at 50 °C

and stirred for 12 h. After the color of the mixture was changed from dark purplish green to dark brown, it was then cooled with 400 ml of ice before adding 3 ml of H_2O_2, resulting in a color change to a bright yellow. Centrifugation was performed with 200 ml of pure water, 200 ml of 30% HCl and 200 ml of ethanol to separate the resulting graphene oxide. The process was repeated until pH 7. The GO after washing was dried in a vacuum at 60 °C.

2.3. Synthesis of GO-ZnO nanocomposite

The GO solution was prepared by dispersing 2 g of GO into 600 ml of pure water, followed by sonication for 30 min. Subsequently, 100 ml of 0.04 M $ZnCl_2$ (0.544 g) was added dropwise into a GO solution with continuous sonication for 30 min to produce a uniform solution. A 0.0267 M solution of NaOH (300 mL, 0.32 g) was added dropwise to the solution with a vigorous stirring to obtain the GO-ZnO nanocomposite. The GO-ZnO composite was obtained by centrifugation with pure water and ethanol followed by drying (Fig. 1) (Ramadoss and Kim, 2013; Atchudan et al., 2016).

2.4. PVDF and GO-ZnO hybrid membranes fabrication

Table 1 lists the concentration of the components. A mixture of PVP and nanoparticles was prepared using a certain quantity of nanoparticles (GO or GO-ZnO) in NMP with ultrasonication for 3 h. PVDF was then placed in the mixture with stirring well for 24 h at 80 °C to obtain the cast solution. After stirring, the solutions were sealed and stored at room temperature for up to 9 h to remove the bubbles. The solution was then cast on a glass plate using a casting knife and immersed immediately into a water coagulating bath at room temperature. After complete coagulation, a flat sheet membrane was peeled off from the glass plate and stored in distilled water until required.

2.5. Characterizations of nanoparticles

The chemical compositions on the GO and GO-ZnO were determined by FTIR spectroscopy (Alpha Bruker FTIR) by recording scan range from 400 cm to 1 to 4000 cm-1. XPS (K-Alpha, Thermo Scientific, UK) was performed using monochromated Al Kα radiation with a spot size of 400 μm, and a pass energy of 30 eV to examine the functionalized group and of zinc, oxygen, and carbon composition in the nanomaterials. The XPs spectrum was analyzed using Thermo Scientific™ Avantage software (version 5.932). The crystal structure of the nanocomposites was investigated by XRD, and SEM (S-4800, Hitachi, Japan) was used to observe the morphology of the GO and GO-ZnO nanomaterials.

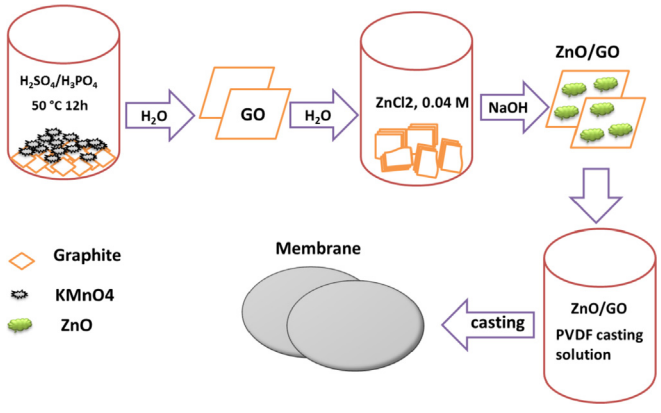

Fig. 1. Schematic diagram of the process for fabricating the GO-ZnO nanoparticles and membranes.

Table 1
Compositions of the casting solution: PVDF, PVP, and GO, GO-ZnO.

Membrane code	NMP (%)	PVDF (%)	PVP (%)	Nanocomposite	
				GO (%)	ZnO-GO (%)
M0	82	17	1	–	–
M1	82	17	1	0.1	–
M2	82	17	1	0.125	–
M3	82	17	1	0.15	–
M4	82	17	1	–	0.1
M5	82	17	1	–	0.15
M6	82	17	1	–	0.2
M7	82	17	1	–	0.3

2.6. Characterization of the membranes

The membrane microstructures, top surface, and cross-section were examined by SEM (S-4800, Hitachi, Japan). All membranes were coated with a thin platinum layer to reflect the X-ray beam in SEM.

2.6.1. Water contact angle (CA) measurements, porosity and mean pore size calculation, and rejection measurements

The contact angle of the droplet with the membrane surface was determined by placing a water droplet on the membrane surface, and measuring the angle using an Apollo 9000 Contact Angle Analyzer. To obtain the most precise results, the angle was measured at five different locations on the membrane and the average results were obtained. The proportion of the volume of pores and the total volume of the membrane is called the membrane porosity, ε (%). The porosity was determined by dividing the volume of liquid contained in the membrane pores by the volume of the membrane, as defined in the following equation (J. Zhang et al., 2013):

$$\varepsilon = \frac{\omega 1 - \omega 2}{A \times l \times dw} \times 100\%$$

where ω1 denotes the wet membrane weight; ω2 denotes the dry membrane weight; A denotes the membrane effective area (m^2); dw denotes the water density (0.998 g cm^{-3}); and l denotes the membrane thickness (m).

The membranes mean pore size (r_m) were determined using the Guerout- Elford-Ferry equation:

$$r_m = \sqrt{\frac{(2.9 - 1.75\varepsilon) \times 8\eta l Q}{\varepsilon \times A \times P}}$$

where η is the deionized water viscosity (8.9 × 10-4 Pa s); Q is the permeation volume of deionized water per unit time ($m^3 \cdot s^{-1}$); and P is the operating pressure (Pa) (Ayyaru and Ahn, 2017).

A rejection test was performed with a BSA solution (0.5 g/l in a phosphate buffer solution (PBS) at pH 7.0). The pure water was altered to a BSA solution. The concentration of BSA in the feed and permeation solution was determined using a UV-spectrophotometer. The rejection was defined using the following equation:

$$R = \left(1 - C_p / C_f\right) \times 100\%$$

where C_p and C_f denote the protein concentration in the permeate and feed solutions, respectively.

2.6.2. Water flux and anti-fouling test

The water flux was examined by cross-flow filtration system through the membrane (a 6 cm inner diameter and a 28.26 cm^2 effective area) at 25 °C. The cross-flow filtration was connected to a feed tank with a pump as described in previous studies (Ayyaru and Ahn, 2017; Ayyaru et al., 2018). Inlet and outlet valves were used to control the feed pressure. The filtrate was launched at 0.2 Mpa during 30 min for pre-compaction of the membranes and the operating pressure was restored at 0.1 MPa. To minimize the investigation error, four samples of each type of membrane were investigated, and the average was calculated. The following equation was used to calculate the water flux, J_{w1} (L m^{-1} h^{-1}) (Zhao et al., 2012):

$$J_{W1} = \frac{V}{A\Delta t}$$

where V (L) denotes the permeated water volume; A (m^2) denotes the membrane area, and Δt (h) denotes the permeation time. In order to conform the membrane stability of the prepared membranes the flux test was performed using deionized water for 10 days after reaching the stable flux.

Three phases occur during the anti-fouling experiments. The first phase was pure water filtration, which was run for 60 min. The next phase was also run for 1 h, but pure water was altered using a 0.5 g/l BSA solution. The last one is membrane cleaning in a cross-flow manner with pure water (30 min) and the pure water flux is measured again for another 60 min. These steps are repeated in a cyclic manner for four times, the fourth cycle result was taken for comparison the antifouling properties of the membrane. The flux recovery ratio (FRR), total fouling ratio (Rt), reversible fouling ratio (Rr), and irreversible fouling ratio (Rir) is representative of the anti-fouling effects of the membrane, and these values were calculated using the following equations:

$$FRR = \frac{Jw2}{Jw1} \times 100\%$$

$$R_t = \left(1 - J_p/J_{w1}\right) \times 100\%$$

where *Rt* is the total flux loss caused by total fouling.

$$R_r = \frac{(Jw2 - Jp)}{Jw1} \times 100\%$$

$$R_{ir} = \frac{(Jw1 - Jw2)}{Jw1} \times 100\%$$

where J_{w1} denotes the water flux (L m^{-1} h^{-1}); J_{w2} denotes the water flux of the cleaned membrane (L m^{-1} h^{-1}) and J_p denotes the protein solution flux (L m^{-1} h^{-1}).

2.7. Membrane fouling resistance flux test using activated sludge

The membrane fouling resistance and flux test were performed with real activated sludge in the best composite membranes and bare PVDF membrane. The activated sludge was collected from a municipal wastewater treatment plant (gyeongsan city, South Korea), which has 2500 mg mixed liquor suspended solids (MLSS). The fouling resistances were studied to estimate the effectiveness of the GO-ZnO in membrane using activated sludge as a foulant. The total resistance of the membrane (R_t) can be derived from the sum of several resistances given by Darcy's equation as follows:

$$R_t = R_m + R_c + R_p = \frac{TMP}{\eta J} \quad (1)$$

The fouling individual resistances were calculated, as described elsewhere (Meng et al., 2006). (1) R_m, membranes hydraulic resistance, were calculated by measuring the flux of pure water through a clean membrane. (2) R_t was calculated using the permeate flux of the activated sludge fouled membrane. (3) The membrane was then flushed with pure water and cleaned by removing the gel layer. Subsequently, the DI water flux was measured again to determine the resistance of the pore blocking resistance (R_p) by R_p - R_m, and cake resistance (R_c) can be calculated as $R_c = R_t - (R_m + R_p)$. The flux was measured for up to 400 min. Every 60 min, the membrane was cleaned (back wash) for 10 min. The effluent quality was measured by turbidity units (NTU) and MLSS.

3. Results and discussion

3.1. GO-ZnO nanocomposite characterization

3.1.1. XRD

Fig. 2 shows the XRD pattern of GO, ZnO, and GO-ZnO nanocomposite. The XRD pattern of GO revealed three strong peaks: two peaks at 42.57° and 11.99° 2θ corresponding to (100) and (001) planes, respectively, for GO. In addition, a strong peak at 25.54°, corresponding to the (002) plane, was formed by a redundant part of graphite after fabrication. The wurtzite hexagonal structure of a ZnO crystal was observed in the XRD pattern with a (101) preferred orientation. The peaks at 31.3°, 34.1°, 35.8°, 47.2°, 56.2°, 62.5°, and 67.6° 2θ were assigned to the (100), (002), (101), (102), (110), (103), and (112) planes for ZnO, respectively. These peaks also appeared at the XRD pattern of GO-ZnO and a weak peak at 11.99° 2θ was also noted. This confirms that the GO-ZnO nanocomposite had been synthesized successfully.

3.1.2. FTIR

FTIR spectroscopy (Fig. 3) of these nanocomposite was performed to reveal the functional groups of the synthesized ZnO, GO, and GO- ZnO nanocomposite. The FTIR spectrum of ZnO revealed

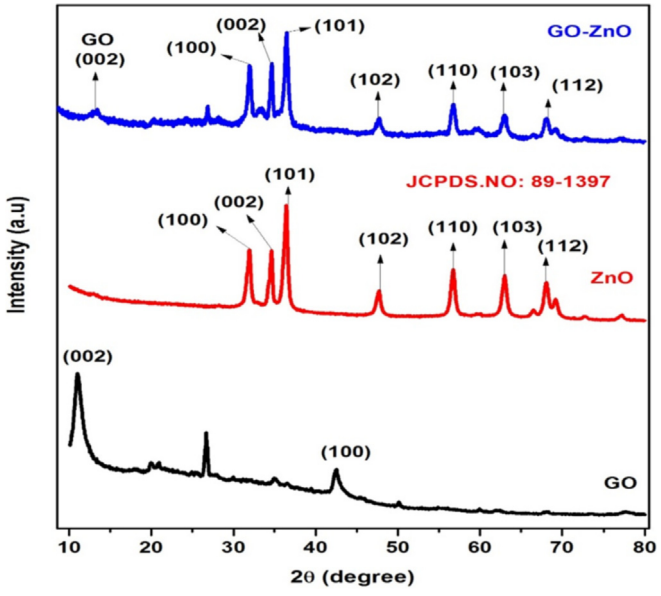

Fig. 2. XRD pattern of GO-ZnO, ZnO and GO.

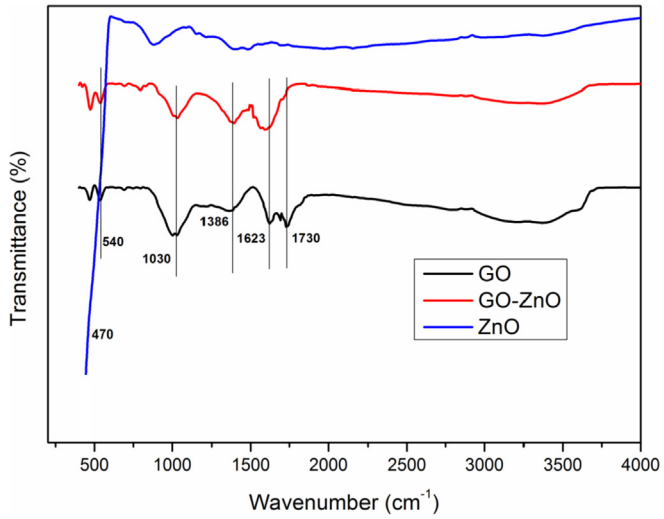

Fig. 3. FTIR spectrum of GO-ZnO, ZnO and GO.

stretching vibrations at below 500 cm^{-1}. This suggests that the synthesized ZnO nanoparticles were pure. The FTIR spectrum of the GO powder revealed absorption bands at 1730 cm^{-1} and 1386 cm^{-1} were assigned to the stretching vibrations of C═O and C–O, respectively (Gondal et al., 2009). The absorption band at 1623 cm^{-1} was assigned to the C═C stretching vibration (sp2-hybridized carbon atoms) (Gondal et al., 2009). The symmetric stretching, asymmetric stretching and deformation vibrations at 1386, 1030, and 540 cm^{-1} indicated the appearance of epoxy groups. The broad absorption band at 3100–3400 cm^{-1} confirmed the presence of the O–H stretching vibration of the absorbed water molecules over the synthesized materials. The FTIR spectrum of the GO- ZnO nanocomposite showed the similarity of many absorption bands to the GO spectrum. On the other hand, the intensity of these band on the FTIR spectrum of GO-ZnO powder was lower than that on the GO powder. This might be explained by the cover of ZnO nanoparticles on the graphene oxide layers. In addition, bonds formed between the functional groups and ZnO in the synthesis process. A weak absorption band observed below 470 cm^{-1} on the FTIR spectrum confirmed the existence of Zn–O stretching vibrations (Gondal et al., 2009). The weak intensity of this absorption band might be due to graphene layers constructed finely over the ZnO nanoparticles.

3.1.3. XPS

XPS is an important tool for examining the chemical state, functionality and composition of a surface. Fig. 4(a) shows the XPS survey result of synthesized GO-ZnO nanoparticles. The spectrum revealed four binding energy peaks at 286.5, 532.6, 1025.3, and 1045.7 eV, which correspond to carbon (C 1 s), oxygen (O 1 s), zinc (Zn $2p_{3/2}$), and zinc (Zn $2p_{1/2}$), respectively. In addition, the spectrum revealed three minor binding energy peaks assigned to Zn 3d, Zn 3p, and Zn 3s. Fig. 4 (b) shows the high resolution XPS spectrum of the C1s level at 284.5 eV, which correspond to C–C and C═C functional groups.

The XPS spectrum of the O1s level in Fig. 4c revealed a peak at 532.36, indicating the appearance of C–OH and Zn–OH functional groups on the surface of the graphene oxide layers (Kumar et al., 2013; Edison et al., 2016). Fig. 4d (Zn2p) revealed two major peaks at 1022.4 and 1045.6 eV, which were assigned to $Zn2p_{3/2}$ and $Zn2p_{1/2}$ levels, respectively. This shows that ZnO is present on the graphene oxide structure (Pawar and Lee, 2014). XPS also revealed 26.4% carbon, 50.3, oxygen, and 23.3% zinc in the synthesized GO-ZnO nanocomposite, respectively. Therefore, the synthesized nanocomposite was highly pure under the preparation conditions.

3.1.4. SEM

Fig. 5 presents SEM images of GO (a,c) and GO-ZnO (b,d) nanocomposites with different magnifications. The SEM image of the GO nanocomposite revealed a single layer structure or 2D structure, which is a feature of GO (Marcano et al., 2010). These layers were individual and had different orientations. This confirmed that the synthesis of GO had been successful. The 2D structure of GO resulted in extremely high physical and chemical activities that are expected to improve the characteristics of the PVDF membrane. On the other hand, ZnO would make the GO more hydrophilic. In contrast, GO also had a reversible impact on ZnO, which can help ZnO exist as discrete particles. SEM images of GO-ZnO revealed ZnO crystals with a rice-like nanostructure scattered on the GO layer (Kim et al., 2017). In addition, the figure also showed that the separated ZnO crystals were bound firmly to the surface of GO layers. This is evidence of the success of the synthesis of the GO-ZnO nanocomposite.

3.2. PVDF and GO-ZnO PVDF membranes characterization

3.2.1. SEM

SEM is an important technique for observing the morphology and structure of a membrane. Fig. 6 shows a cross-section of the various composite membranes and PVDF membrane. All membranes observed a typical asymmetric structure with a clear skin layer and porous sub-layer in the cross-section morphology of membranes. The porous sub-layer accountable for providing mechanical strength and the skin layer is comparatively thin and compact which can make high hydraulic resistance and low flux (Ayyaru and Ahn, 2017). The strong changes observed in thin-layer and sub-layer between the porous structures of the pure PVDFmembrane and modified membrane. Particularly, the 0.2 wt% GO-ZnO/PVDF membrane (M6) membrane of sub-layers were wider and longer that those of the others. This confirmed that the 0.2 GO-ZnO/PVDF membrane has the highest porosity. Thus, due to the fast exchange of solvent and non-solvent in the phase inversion process due to the hydrophilic nanocomposite (Zhang et al., 2013).

Fig. 7. Shows the plan-surface morphology of pure PVDF membrane and modified membranes. The pore structure has been influenced by the incorporation of GO and GO-ZnO nanomaterials to the polymer matrix. When comparing to PVDF the modified membranes showed high pore density and pore size attribute to fast demixing of solvent from polymer solution by nanoparticles during phase inversion (Ji et al., 2011). Fascinatingly, the 0.2 wt% GO-ZnO/PVDF membrane (Fig. 7 M6) exhibits denser pores and large pore size than 0.125 wt% GO/PVDF membrane. This may be due to the better hydrophilicity of GO-ZnO can make the good solvent diffusion from the polymer matrix to non solvent (water), which may facilitate the formation of a larger pore density.

The three-dimensional surface AFM images and mean surface roughness of the membranes showed in Fig. 8. The mean roughness of the PVDF, PVDF-GO (M2), and PVDF-GO/ZnO (M6) membranes were 26.8, 32.9 and 73.5 nm, respectively. The composite membranes showed high surface roughness than that of the PVDF membrane. In particular, the addition of the GO/ZnO showed tremendous improvement in mean roughness than other membranes which may be due the high hydrophilic of GO/ZnO membrane (see contact angle of M6 in Fig. 9). The increased hydrophilicity increases the membrane surface unevenness signifies enlargement of the effective membrane surface area. This can be explained that GO-ZnO nanoparticles completely mixing in dope solution and makes faster coagulation during the phase inversion

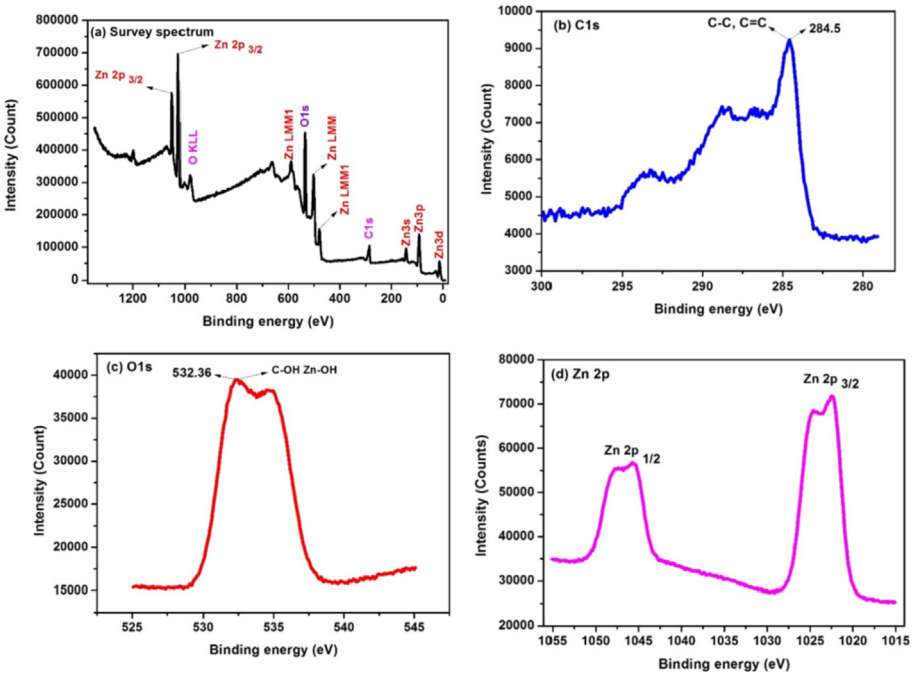

Fig. 4. XPS spectrum of GO-ZnO nanoparticle.

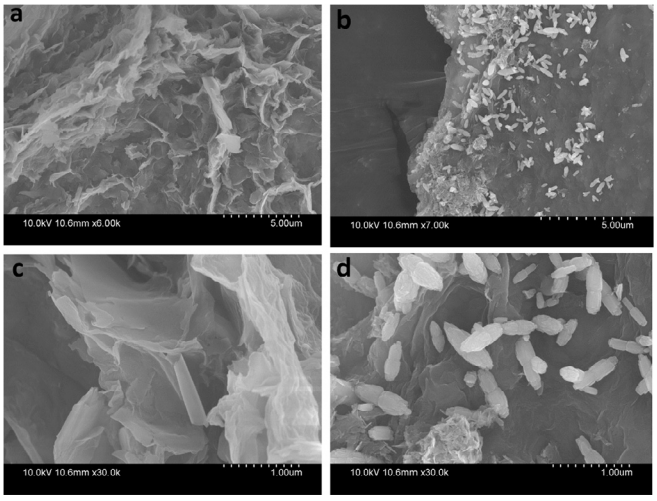

Fig. 5. SEM images of GO and GO-ZnO.

process (Ayyaru and Ahn, 2017), which in turn increased membrane surface area and longer finger-like pores (Fig. 8 M6). The membranes with GO-ZnO are expected to have improved fluxes compared to PVDF membranes and GO membrane (Mahlangu et al., 2017b).

3.2.2. *Water contact angle (CA), porosity, pore size, and rejection measurements*

The contact angle is one of the important methods for characterizing the hydrophilicity of the membrane surface. The contact angle results revealed differences between the PVDF membrane and modified PVDF membranes, as shown in Fig. 9a. The PVDF membrane had the highest contact angle highlighting its hydrophobic nature (Ayyaru and Ahn, 2017). The blend with hydrophilic GO-ZnO membranes, upon increasing the concentration the contact angles of the membranes have been decreased. Thus confirming the findings of other studies (Wu et al., 2014; Mahlangu et al., 2017b). This would explains the high pure water permeability of the membranes with GO-ZnO which also increased with GO-ZnO concentration as observed by other research (Ayyaru and Ahn, 2017; Mahlangu et al., 2017a). The lowest contact angle belongs to 0.2 GO-ZnO/PVDF (M6) membrane (49.8°), whereas the 0.125 GO/PVDF membrane (M2) gained only 52.36°. This confirmed the more positive effect of GO-ZnO compared to GO on the PVDF membrane toward the hydrophilic improvement (Yang et al., 2017). On the other hand, some influencing (agglomeration of nanoparticles in polymer matrix) factors might cause a decrease in the effects of GO-ZnO at a high content in the PVDF membrane matrix.

The diagram (Fig. 9a) showed the effects of the different additives on the porosity of PVDF membranes. The porosity range of the different membranes ranged from 51.28% to 66.07%; 51.28% belongs to the bare PVDF membrane. This suggests that the hydrophilic additives in the polymer matrix can be the cause of the rapid exchange of solvent and non-solvent in the phase inversion process. As a result, the porosity of these membranes was enhanced. The improvement impacted directly on the roughness and water flux of the membranes. On the other hand, some problems, such as the agglomeration of nanoparticles in the polymer solution when a large number of additives is supplemented on the solution, might thicken the sub-layer of 0.3 wt% GO-ZnO/PVDF membrane (Fig. 6 M7) (Yang et al., 2017). This also occurred on the 0.15 wt% GO/PVDF (M3) membrane. This may be due to the large increased in the viscosity of the casting solution and the agglomeration of nanoparticles with the dispersion of excess.

Fig. 9b shows that all BSA rejection of the membranes ranged from 86% to 93%. This expressed the high BSA removal capacity of all membranes. The addition of GO-ZnO improved BSA rejection and rejection increased with increasing GO-ZnO concentration. This can also be attributed to improvement in repulsive non-electrostatic interactions between the membranes and foulant (Ayyaru and Ahn, 2017; Mahlangu et al., 2017a). BSA has a negative charge at neutral pH therefore, it is highly possible to repulse the negative charge membrane (GO-ZnO) towards the negative charge

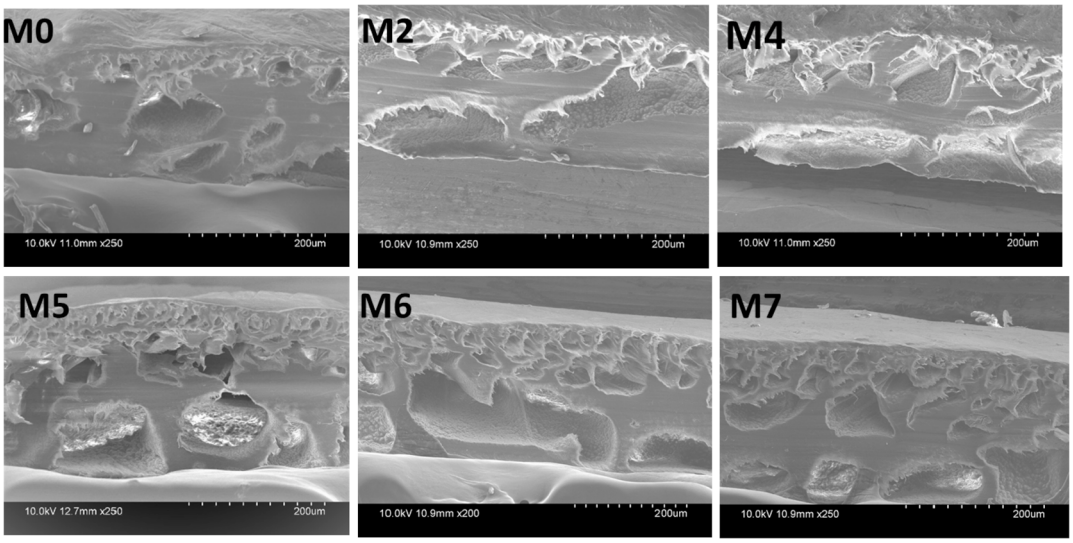

Fig. 6. Cross section SEM images of different membranes.

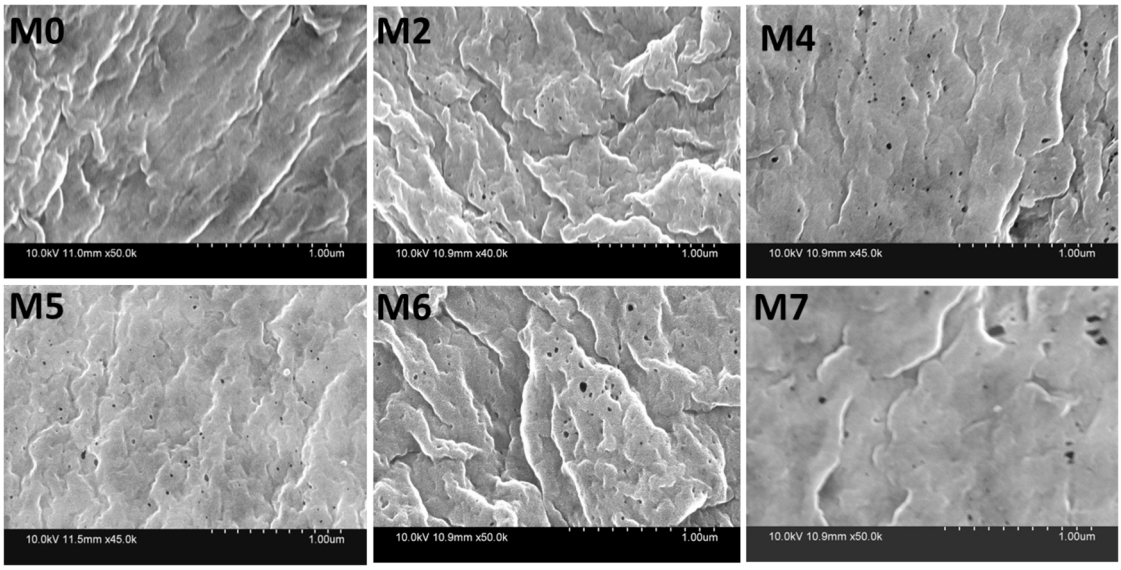

Fig. 7. Plan view SEM images of all types of membranes.

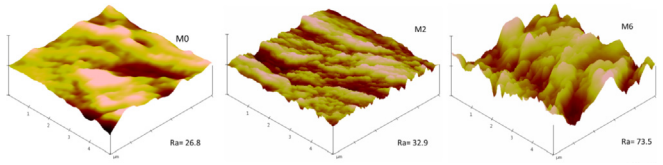

Fig. 8. AFM images and roughness of PVDF (M0), PVDF-GO (M3), PVDF-GO/ZnO (M6) membranes.

foulant (Ayyaru and Ahn, 2017). With BSA molecular weight cut-off (MWCO) of 66 000 Da, the membranes belong to the ultrafiltration range. Fig. 9b shows the pore sizes of all membranes. It was observed, that when increasing the concentration of nanoparticles the pore sizes were increased (excluding M3 and M7). At 0.2 wt % GO-ZnO (M6), the mean pore size reached 43 nm, which was 22.8% higher than that of the bare PVDF membrane (M0). The porosity data also showed a similar trend with pore sizes of membranes. The pore sizes of membranes further confirmed that all membranes belong the ultrafiltration range. The high pore size membrane (M6) exhibited high rejection which might be due to their great hydrophilicity or low contact angle. In contrast, the low pore size PVDF membrane showed less rejection, which can be attributed to the hydrophobic nature of the PVDF membrane.

3.2.3. *Water flux and anti-fouling performance*

Permeability is one of the most important characteristics to assess the quality of a membrane and can be evaluated by the water flux and anti-fouling properties. The water flux of a membrane can be affected by the appropriate additives used in membrane production. Fig. 10a compares the water flux of different additives in the PVDF membrane structure. The M6 membrane (0.2 wt % of GO-ZnO) contributed to the highest water flux (170.73 l/m^2.h) than PVDF-GO M3 and PVDF membrane. The association of ZnO and GO with the PVDF membrane not only increases the permeability of the PVDF membrane, but also improves the hydrophilicity of GO,

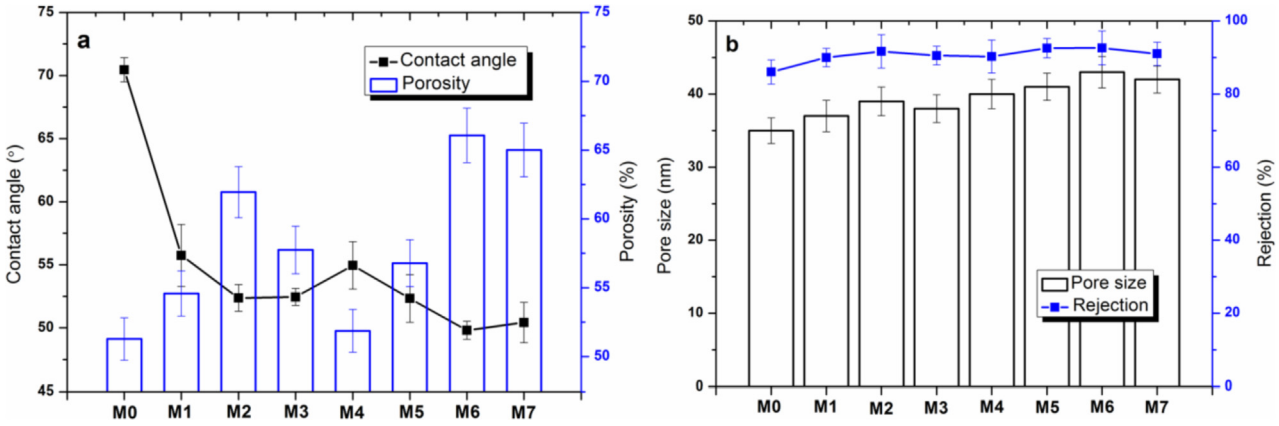

Fig. 9. Chart of the contact angle and porosity (a) and rejection and pore sizes of all membranes (b).

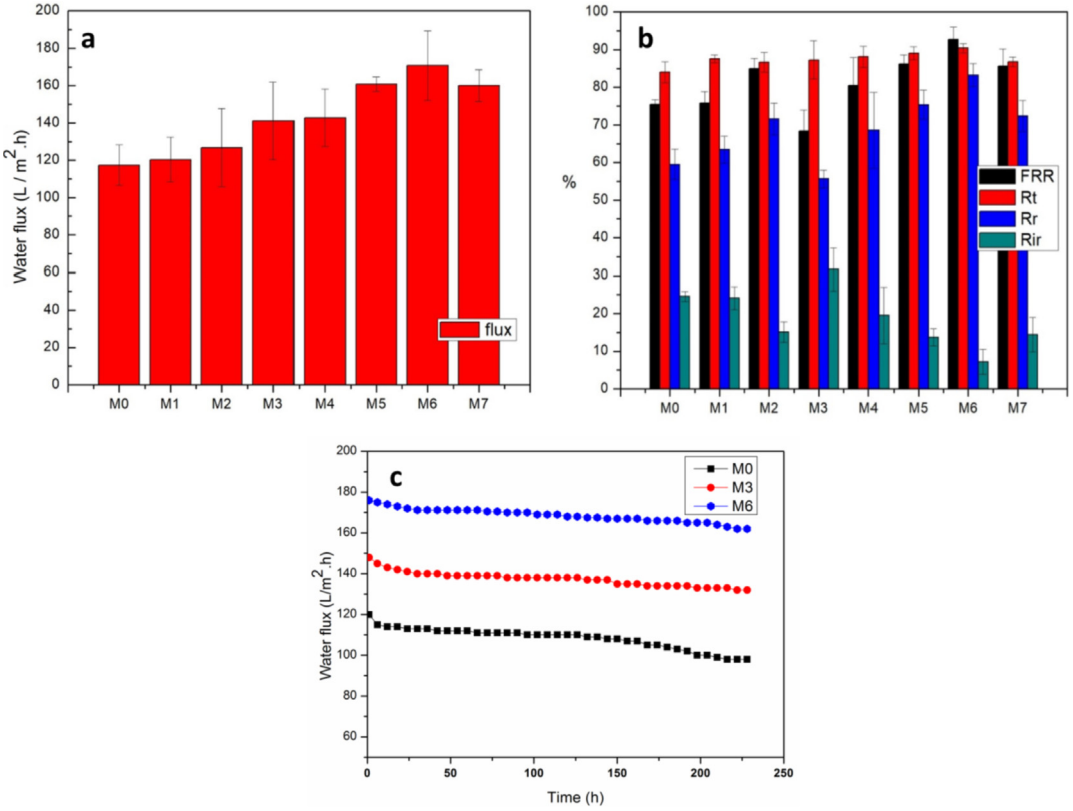

Fig. 10. Water flux of all types of the membranes (a), anti-fouling properties of all types of membranes (b) and long time deionize water flux of PVDF (M0), PVDF-GO (M3), PVDF-GO/ZnO (M6) membranes (C).

which is an amphiphilic material. The ZnO crystals on the GO strengthen the hydrogen-bonding (due to the hydroxyl group of Zn−OH) with water, thus make dense water layer, which allows water to pass easily through the membranes (Ayyaru and Ahn, 2017). In addition, the larger pore size of the GO-ZnO/PVDF membranes provides water more opportunities to permeate through the membrane pores. Fig. 10c shows long duration flux with deionized water for PVDF M0), PVDF-GO M3, PVDF-GO/ZnO (M6). All the membrane exhibited stable flux for a long time (224 h) (only 5% flux decline), which indicates that the prepared membranes had a good mechanical strength. Moreover, the longtime flux result of composite membranes conforms that stability of GO and GO-ZnO in PVDF membrane without leaching.

The antifouling properties can be evaluated using the calculated flux recovery ratio (FRR), total fouling ratio (R_t), reversible fouling ratio (R_r), and irreversible fouling ratio (R_{ir}). These values indicate the existence of anti-fouling behaviors on the membrane during filtration. Fig. 10b shows that the pure PVDF membrane and 0.15 GO/PVDF membrane (M3) have the lowest results compared to the others, which suggests that the natural hydrophobicity of PVDF attracted more hydrophobic foulant in the BSA solution. On the other hand, 0.15 GO/PVDF showed a strong decrease in anti-fouling properties because of the agglomeration of nanoparticles. On the other hand, the membrane modified by GO gained positive improvement at a content of 0.125 wt % in the PVDF membrane, with a FRR, R_t, R_r and R_{ir} of 84.9%, 86.67%, 71.58%, and 15.09%

Table 2
Fouling resistances activated sludge for PVDF, PVDF-GO (M3) and PVDF-GO-ZnO (M6) membranes.

Membrane resistance ($\times 10^8\ m^{-1}$)	PVDF membrane	Nanocomposite membrane	
		PVDF-GO (M3)	PVDF-GO-ZnO (M6)
R_m	31.2	25.6	21.2
R_p	21.7	6.4	1
R_c	36.3	31.6	29.6
R_t	89.2	63.6	51.8

respectively. In addition, significant improvement was observed in the anti-fouling parameters of the PVDF membranes modified with GO-ZnO. These results indicate that the PVDF membrane with 0.2 wt % of GO-ZnO enhanced the anti-fouling ability of the membrane compared to the other GO/PVDF and bare PVDF membranes. The supplement of GO-ZnO in the polymer structure is believed to build a thicker water hydrogen layer, preventing foulants binding to membrane surface and pores. The PVDF membrane containing 0.2 wt % of GO-ZnO gave the highest FRR (92.79%) and highest R_r (83.21%) and lowest R_{ir} (only 7.21%)

3.2.4. Fouling resistance analysis and flux test performance using activated sludge

Fouling of membrane in membrane bioreactor (MBR) can be categorized by an outer cake layer on the membrane surface and an inner gel layer in the membrane. Cake layer from MLSS, that contributes to reversible fouling resistance R_c, can be removed by a strong shear force or backwashing. The inner gel layer formed by strongly attached soluble microbialpolymer (SMP) or EPS clogs pores and blocks and contributes to the irreversible fouling resistance (R_p) that can only be removed by chemical cleaning (Zhao et al., 2014). Table 2 shows the resistance of composite membranes (M3, M6) and PVDF membrane (M0). The results reflect that the nanoparticles impact the surface resistance of R_p and R_t. The cake layer observed was dominant in the total resistance of all membranes (57.1, 49.6 and 40.6% for PVDF-GO-ZnO, PVDF-GO and PVDF respectively), which due the deposition of activated sludge on the membranes (MLSS). Membrane resistance of (R_m) of PVDF-GO-ZnO and PVDF-GO composite membranes exhibited low than the PVDF membrane, suggest that blending of nanoparticles can improve the PVDF hydrophilicity (Zhao et al., 2014). The R_p of the membranes caused by pore clogging and irreversible fouling, although R_p contributed less to the total resistance (R_t), it can be caused significant decline of permeation flux with long time and reduce the lifetime of membranes (Maximous et al., 2009). The R_p of PVDF-GO/ZnO composite membrane showed very low compare to both membranes (1/6 and 1/22 for PVDF-GO and PVDF membrane, respectively), indicates that the introduction of GO-ZnO improved the surface characteristics of PVDF membrane when compared to addition of GO, which suggest that GO-ZnO has more hydrophilic nature than GO. Which in turn increases the antifouling properties of GO-ZnO composite membrane attributable to the

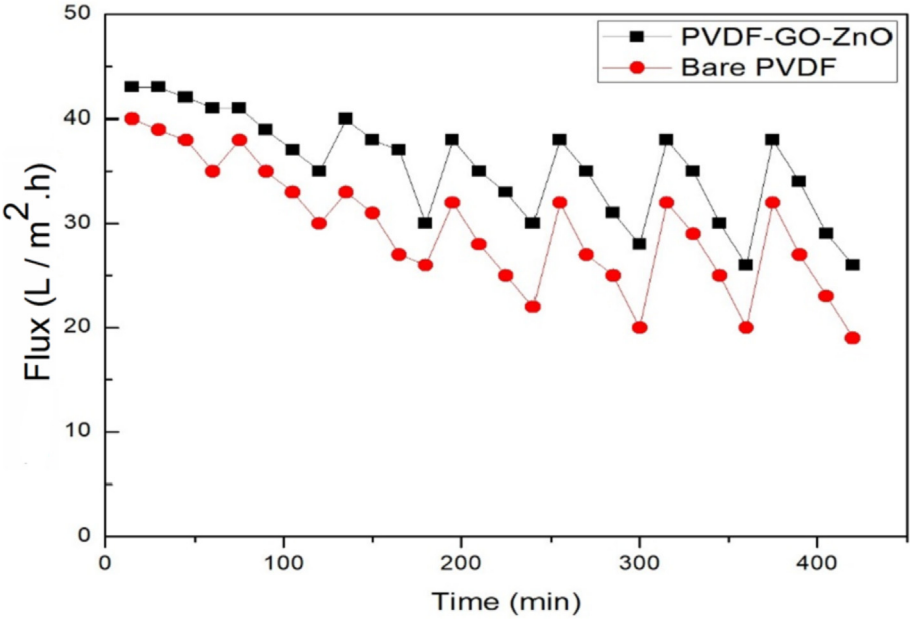

Fig. 11. Flux test using activated sludge.

Table 3
Comparative performance of the hybrid nanocomposite membranes of other studies.

Type	Water flux (L m^{-2} h^{-1})	Content of additives (%)	Rejection (%)	References
PSf-GO	240	–	96	Wu et al. (2014)
PSf-GO/SiO_2	380	0.3	97	Wu et al. (2014)
PVDF-GO	81.95 (±1.20)	0.05	96.5 ± 2.1	Safarpour et al. (2015)
PVDF-GO/TiO_2	221	0.05	99	Safarpour et al. (2015)
PES-GO-ZnO	7.8 ± 0.8	0.05	90 (Atrazine)	Mahlangu et al. (2017b)
PES-GO	2.6 ± 0.1	0.0125	53 (Atrazine)	Mahlangu et al. (2017b)
PVDF-GO	120	0.125	91	This work
PVDF-GO/ZnO	170.73	0.2	92	This work

reduction in hydrophobic interaction between the hydrophilic membrane (PVDF-GO/ZnO) and foulants (Maximous et al., 2009) (see Table 3).

Fig. 11 shows the results of the flux test using activated sludge. The activated sludge flux test was performed with the best hybrid membrane 0.2 wt % GO-ZnO/PVDF (M6) and bare PVDF membrane. A decreasing trend in both membranes was observed over time, but the membrane containing GO-ZnO in the polymer matrix had a higher flux and its decreasing trend was lower than that of the bare PVDF membrane. This confirmed the performance of adding GO-ZnO to the PVDF membrane structure. The MLSS concentrations in the effluent were almost zero (data not shown) and the turbidity of the effluent in the nanocomposite membrane was 0.6 NTU during the test. In addition, the effluent quality after the composite membrane was stable, indicating that the composite membrane can be used for practical applications.

Table 3 lists the highest water flux and rejection of all the nanocomposite membranes in comparison with the GO membrane (Wu et al., 2014; Safarpour et al., 2015; Mahlangu et al., 2017b). Similarly, the present study also revealed the same. This confirmed that the association of GO and metal oxides improved the water flux and anti-fouling ability of the membranes. Mahlangu et al., examine the PES membranes modified with GO-ZnO for trace organic compounds (TOrCs) of wastewater (Mahlangu et al., 2017b). The result of water flux of membrane was very low when compared to those reported in the literature for microfiltration and ultrafiltration membranes. This may be due the membrane synthesis approach of double-casting phase inversion (DCPI) method.

4. Conclusion

For the membrane, the improvement of permeability, high hydrophilicity and enhanced antifouling performance are the positive effects of blending additives into the membrane structure matrix. The association between ZnO and GO in this study was harnessed to produce a new additive for the PVDF membrane. The GO-ZnO/PVDF membrane was fabricated using the phase inversion process. The characteristics of the membranes were analyzed by SEM, porosity measurements, hydrophilicity analysis, and filtration experiments. The CA of the PVDF membrane was improved significantly when blended with 0.2 wt% of GO-ZnO (49.8°). The porosity of this membrane was 66.07%. The antifouling properties of this membrane were 92.79% (FRR), 83.21% (R_r), and 7.21% (R_{ir}). These parameters showed the positive effects of additives on the PVDF membrane. In addition, high flux was observed in the GO-ZnO/PVDF membrane using activated sludge and excellent effluent quality was also maintained. These effects were explained by the higher hydrophilicity due to the association of ZnO and GO in the PVDF structure matrix.

Acknowledgement

This study was supported partly by the Yeungnam University Research Grant.

References

Atchudan, R., Edison, T.N.J.I., Perumal, S., Karthikeyan, D., Lee, Y.R., 2016. Facile synthesis of zinc oxide nanoparticles decorated graphene oxide composite via simple solvothermal route and their photocatalytic activity on methylene blue degradation. J. Photochem. Photobiol. B Biol. 162, 500–510.

Ayyaru, S., Ahn, Y.-H., 2017. Application of sulfonic acid group functionalized graphene oxide to improve hydrophilicity, permeability, and antifouling of PVDF nanocomposite ultrafiltration membranes. J. Membr. Sci. 525, 210–219.

Ayyaru, S., Ahn, Y.-H., 2018. Fabrication and separation performance of polyethersulfone/sulfonated TiO2 (PES–STiO2) ultrafiltration membranes for fouling mitigation. J. Ind. Eng. Chem. 67, 199–209.

Ayyaru, S., Dharmalingam, S., 2011. Development of MFC using sulphonated polyether ether ketone (SPEEK) membrane for electricity generation from waste water. Bioresour. Technol. 102, 11167–11171.

Ayyaru, S., Choi, J., Ahn, Y.-H., 2018. Biofouling reduction in a MBR by the application of a lytic phage on a modified nanocomposite membrane. Environ. Sci.: Water Res. Technol. 4, 1624–1638.

Ayyaru, S., Pandiyan, R., Ahn, Y.-H., 2019. Fabrication and characterization of antifouling and non-toxic polyvinylidene fluoride -Sulphonated carbon nanotube ultrafiltration membranes for membrane bioreactors applications. Chem. Eng. Res. Des. 142, 176–188.

Bahng, J.H., Yeom, B., Wang, Y., Tung, S.O., Hoff, J.D., Kotov, N., 2015. Anomalous dispersions of 'hedgehog' particles. Nature 517, 596.

Beydaghi, H., Javanbakht, M., Kowsari, E., 2014. Synthesis and characterization of poly(vinyl alcohol)/sulfonated graphene oxide nanocomposite membranes for use in proton exchange membrane fuel cells (PEMFCs). Ind. Eng. Chem. Res. 53, 16621–16632.

Bottino, A., Capannelli, G., Comite, A., 2002. Preparation and characterization of novel porous PVDF-ZrO2 composite membranes. Desalination 146, 35–40.

Cao, X., Ma, J., Shi, X., Ren, Z., 2006. Effect of TiO2 nanoparticle size on the performance of PVDF membrane. Appl. Surf. Sci. 253, 2003–2010.

Chang, I.-S., Clech, P.L., Jefferson, B., Judd, S., 2002. Membrane fouling in membrane bioreactors for wastewater treatment. J. Environ. Eng. 128, 1018–1029.

Chang, X., Wang, Z., Quan, S., Xu, Y., Jiang, Z., Shao, L., 2014. Exploring the synergetic effects of graphene oxide (GO) and polyvinylpyrrodione (PVP) on poly(-vinylylidenefluoride) (PVDF) ultrafiltration membrane performance. Appl. Surf. Sci. 316, 537–548.

Cui, A., Liu, Z., Xiao, C., Zhang, Y., 2010. Effect of micro-sized SiO2-particle on the performance of PVDF blend membranes via TIPS. J. Membr. Sci. 360, 259–264.

Edison, T.N.J.I., Atchudan, R., Shim, J.-J., Kalimuthu, S., Ahn, B.-C., Lee, Y.R., 2016. Turn-off fluorescence sensor for the detection of ferric ion in water using green synthesized N-doped carbon dots and its bio-imaging. J. Photochem. Photobiol. B Biol. 158, 235–242.

Feng, K., Tang, B., Wu, P., 2013. "Evaporating" graphene oxide sheets (GOSs) for rolled up GOSs and its applications in proton exchange membrane fuel cell. ACS Appl. Mater. Interfaces 5, 1481–1488.

Feng, K.T., Beibei, wu, Peiyi, 2014. Sulfonated graphene oxide-silica for highly selective nafion-based proton exchange membranes. J. Mater. Chem. 2, 16083–16092.

Gondal, M.A., Drmosh, Q.A., Yamani, Z.H., Saleh, T.A., 2009. Synthesis of ZnO2 nanoparticles by laser ablation in liquid and their annealing transformation into ZnO nanoparticles. Appl. Surf. Sci. 256, 298–304.

Howe KJ, C.M., 2002. Fouling of microfiltration and ultrafiltration membranes by natural waters. Environ. Sci. Technol. 36, 3571–3576.

Huang, Z.-Q., Zheng, F., Zhang, Z., Xu, H.-T., Zhou, K.-M., 2012. The performance of the PVDF-Fe3O4 ultrafiltration membrane and the effect of a parallel magnetic field used during the membrane formation. Desalination 292, 64–72.

Ji, J., Zhang, G., Chen, H., Wang, S., Zhang, G., Zhang, F., Fan, X., 2011. Sulfonated graphene as water-tolerant solid acid catalyst. Chem. Sci. 2, 484–487.

Jiao, L., Zhang, L., Wang, X., Diankov, G., Dai, H., 2009. Narrow graphene nanoribbons from carbon nanotubes. Nature 458, 877.

Kim, S., Jinschek, J.R., Chen, H., Sholl, D.S., Marand, E., 2007. Scalable fabrication of carbon nanotube/polymer nanocomposite membranes for high flux gas transport. Nano Lett. 7, 2806–2811.

Kim, S.-W., Lee, S., Saqib, A.N.S., Lee, Y.H., Jung, M.-H., 2017. Ferromagnetism in undoped ZnO nanostructures synthesized by solution plasma process. Curr. Appl. Phys. 17, 181–185.

Kumar, V., Singh, F., Ntwaeaborwa, O.M., Swart, H.C., 2013. Effect of Br+6 ions on the structural, morphological and luminescent properties of ZnO/Si thin films. Appl. Surf. Sci. 279, 472–478.

Lai, C.Y., Groth, A., Gray, S., Duke, M., 2014. Nanocomposites for improved physical durability of porous PVDF membranes. Membranes 4, 55–78.

Li, B., Liu, T., Wang, Y., Wang, Z., 2012. ZnO/graphene-oxide nanocomposite with remarkably enhanced visible-light-driven photocatalytic performance. J. Colloid Interface Sci. 377, 114–121.

Li, N., Tian, Y., Zhao, J., Kong, L., Zhang, J., Zuo, W., Cui, H., Lin, Q., 2018. Anti-irreversible fouling of precisely-designed PVDF-ZnO membrane: effects of ion strength and co-existing cations. Appl. Surf. Sci. 459, 397–405.

Ma, J., Zhao, Y., Xu, Z., Min, C., Zhou, B., Li, Y., Li, B., Niu, J., 2013. Role of oxygen-containing groups on MWCNTs in enhanced separation and permeability performance for PVDF hybrid ultrafiltration membranes. Desalination 320, 1–9.

Mahlangu, O.T., Nackaerts, R., Mamba, B.B., Verliefde, A.R.D., 2017a. Development of hydrophilic GO-ZnO/PES membranes for treatment of pharmaceutical wastewater. Water Sci. Technol. 76, 501–514.

Mahlangu, O.T., Nackaerts, R., Thwala, J.M., Mamba, B.B., Verliefde, A.R.D., 2017b. Hydrophilic fouling-resistant GO-ZnO/PES membranes for wastewater reclamation. J. Membr. Sci. 524, 43–55.

Marcano, D.C., Kosynkin, D.V., Berlin, J.M., Sinitskii, A., Sun, Z., Slesarev, A., Alemany, L.B., Lu, W., Tour, J.M., 2010. Improved synthesis of graphene oxide. ACS Nano 4, 4806–4814.

Maximous, N., Nakhla, G., Wan, W., Wong, K., 2009. Preparation, characterization and performance of Al2O3/PES membrane for wastewater filtration. J. Membr. Sci. 341, 67–75.

Meng, F., Yang, F., Xiao, J., Zhang, H., Gong, Z., 2006. A new insight into membrane fouling mechanism during membrane filtration of bulking and normal sludge suspension. J. Membr. Sci. 285, 159–165.

Moezzi, A., McDonagh, A.M., Cortie, M.B., 2012. Zinc oxide particles: synthesis, properties and applications. Chem. Eng. J. 185–186, 1–22.
Pawar, R.C., Lee, C.S., 2014. Single-step sensitization of reduced graphene oxide sheets and CdS nanoparticles on ZnO nanorods as visible-light photocatalysts. Appl. Catal. B Environ. 144, 57–65.
Qin, Q., Hou, Z., Lu, X., Bian, X., Chen, L., Shen, L., Wang, S., 2013. Microfiltration membranes prepared from poly(N-vinyl-2-pyrrolidone) grafted poly(vinylidene fluoride) synthesized by simultaneous irradiation. J. Membr. Sci. 427, 303–310.
Ramadoss, A., Kim, S.J., 2013. Facile preparation and electrochemical characterization of graphene/ZnO nanocomposite for supercapacitor applications. Mater. Chem. Phys. 140, 405–411.
Safarpour, M., Khataee, A., Vatanpour, V., 2015. Effect of reduced graphene oxide/TiO2 nanocomposite with different molar ratios on the performance of PVDF ultrafiltration membranes. Separ. Purif. Technol. 140, 32–42.
Wang, Z., Yu, H., Xia, J., Zhang, F., Li, F., Xia, Y., Li, Y., 2012. Novel GO-blended PVDF ultrafiltration membranes. Desalination 299, 50–54.
Warsinger, D.M., Chakraborty, S., Tow, E.W., Plumlee, M.H., Bellona, C., Loutatidou, S., Karimi, L., Mikelonis, A.M., Achilli, A., Ghassemi, A., Padhye, L.P., Snyder, S.A., Curcio, S., Vecitis, C., Arafat, H.A., Lienhard, J.H.t., 2016. A review of polymeric membranes and processes for potable water reuse. Prog. Polym. Sci. 81, 209–237.
Wei, Y., Chu, H.-Q., Dong, B.-Z., Li, X., Xia, S.-J., Qiang, Z.-M., 2011. Effect of TiO2 nanowire addition on PVDF ultrafiltration membrane performance. Desalination 272, 90–97.
Wu, G., Gan, S., Cui, L., Xu, Y., 2008. Preparation and characterization of PES/TiO2 composite membranes. Appl. Surf. Sci. 254, 7080–7086.
Wu, H., Tang, B., Wu, P., 2014. Development of novel SiO2–GO nanohybrid/polysulfone membrane with enhanced performance. J. Membr. Sci. 451, 94–102.
Yan, L., Li, Y.S., Xiang, C.B., Xianda, S., 2006. Effect of nano-sized Al2O3-particle addition on PVDF ultrafiltration membrane performance. J. Membr. Sci. 276, 162–167.
Yang, Y., Wang, P., 2006. Preparation and characterizations of a new PS/TiO2 hybrid membranes by sol–gel process. Polymer 47, 2683–2688.
Yang, L., Liu, L., Wang, Z., 2017. Preparation of PVDF/GOSiO2 hybrid microfiltration membrane towards enhanced perm-selectivity and anti-fouling property. J. Taiwan Inst. Chem. Eng. 78, 500–509.
Zhang, J., ZX, Mai, W., Min, C., Zhou, B., Shan, M., Li, Y., Yang, C., Wang, Z., Qian, X., 2013. Improved hydrophilicity, permeability, antifouling and mechanical performance of PVDF composite ultrafiltration membranes tailored by oxidized low-dimensional carbon nanomaterials. J. Mater. Chem. A 1, 3101–3111.
Zhang, D., Dai, F., Zhang, P., An, Z., Zhao, Y., Chen, L., 2019. The photodegradation of methylene blue in water with PVDF/GO/ZnO composite membrane. Mater. Sci. Eng. C 96, 684–692.
Zhao, X., Ma, J., Wang, Z., Wen, G., Jiang, J., Shi, F., Sheng, L., 2012. Hyperbranched-polymer functionalized multi-walled carbon nanotubes for poly (vinylidene fluoride) membranes: from dispersion to blended fouling-control membrane. Desalination 303, 29–38.
Zhao, C., Xu, X., Chen, J., Wang, G., Yang, F., 2014. Highly effective antifouling performance of PVDF/graphene oxide composite membrane in membrane bioreactor (MBR) system. Desalination 340, 59–66.
Zhao, W., Li, H., Liu, Z., Wang, D., Liu, S., 2018. Controlled defects and enhanced electronic extraction in fluorine-incorporated zinc oxide for high-performance planar perovskite solar cells. Sol. Energy Mater. Sol. Cells 182, 263–271.